Sirtuin 1 regulates pulmonary artery smooth muscle cell proliferation: role in pulmonary arterial hypertension

Giada Zurlo, Jérôme Piquereau, Maryline Moulin, Julie Pires da Silva, Mélanie Gressette, Benoît Ranchoux, Anne Garnier, Renée Ventura-Clapier, Elie Fadel, Marc Humbert, et al.

Sirtuin 1 regulates pulmonary artery smooth muscle cell proliferation: Role in pulmonary arterial hypertension

Running head: Sirtuin1 and pulmonary arterial hypertension

Giada ZURLO[a], Jérôme PIQUEREAU[a], Maryline MOULIN[a], Julie PIRES DA SILVA[a], Mélanie GRESSETTE[a], Benoît RANCHOUX[b], Anne GARNIER[a], Renée VENTURA-CLAPIER[a], Elie FADEL[c], Marc HUMBERT[b], Christophe LEMAIRE[a,d], Frédéric PERROS[b] and Vladimir VEKSLER[a]

[a]INSERM UMR-S1180, Univ. Paris-Sud, Université Paris-Saclay, Châtenay-Malabry, France
[b]Université Paris-Saclay, Faculté de Médecine, 94270 Le Kremlin-Bicêtre, France; AP-HP, hôpital Bicêtre, Service de pneumologie, 94270 Le Kremlin-Bicêtre, France; Centre chirurgical Marie-Lannelongue, INSERM UMR-S 999, 92060 Le Plessis-Robinson, France.
[c]Université Paris-Saclay, Faculté de Médecine, 94270 Le Kremlin-Bicêtre, France; Centre chirurgical Marie-Lannelongue, INSERM UMR-S 999, 92060 Le Plessis-Robinson, France; Centre chirurgical Marie-Lannelongue, Service de chirurgie thoracique, 92060 Le Plessis-Robinson, France.
[d]Univ. Versailles Saint-Quentin en Yvelines, Université Paris-Saclay, Versailles, France

This manuscript, or part of it, never has been published.

This work was supported by INSERM (Institut national de la santé et de la recherche médicale, France) as well as by grants from Laboratory of Excellence LERMIT, FRM (Fondation pour la Recherche Médicale) to AG (#DPM20121125546) and Région Ile de France CODDIM to RVC (#cod110153).
Disclosures: None

Address for correspondence: Pr Vladimir VEKSLER

UMR-S1180, Univ. Paris-Sud, Université Paris-Saclay, Châtenay-Malabry, 5 rue J.-B.Clément, 92296, France
Telephone: (+33) 1 46 83 57 57, Email: Vladimir.veksler@u-psud.fr

Word count: 6557; 7 figures; 1 table, 1 supplementary file

Abstract

Objective: Energy metabolism shift from oxidative phosphorylation towards glycolysis in pulmonary artery smooth muscle cells (PASMCs) is suggested to be involved in their hyperproliferation in pulmonary arterial hypertension (PAH). Here, we studied the role of the deacetylase sirtuin1 (SIRT1) in energy metabolism regulation in PASMCs via various pathways including activation of peroxisome proliferator-activated receptor gamma coactivator-1alpha (PGC-1α), master regulator of mitochondrial biogenesis.

Approach and Results: Contents of PGC-1α and its downstream targets as well as markers of mitochondrial mass (voltage-dependent anion channel and citrate synthase) were diminished in human PAH PASMCs. These cells and platelet derived growth factor-stimulated rat PASMCs demonstrated a shift in cellular acetylated/deacetylated state, as evidenced by the increase of the acetylated forms of SIRT1 targets: histone H1 and forkhead box protein O1 (FOXO1). Rat and human PASMC proliferation was potentiated by SIRT1 pharmacological inhibition or specific downregulation via short interfering RNA. Moreover, after chronic hypoxia exposure, SIRT1 KO mice displayed a more intense vascular remodeling compared to their control littermates, which was associated with an increase in right ventricle pressure and hypertrophy. SIRT1 activator Stac-3 decreased the acetylation of histone H1 and FOXO1 and strongly inhibited rat and human PASMC proliferation without affecting cell mortality. This effect was associated with the activation of mitochondrial biogenesis evidenced by higher expression of mitochondrial markers and downstream targets of PGC-1α.

Conclusions: Altered acetylation/deacetylation balance as the result of SIRT1 inactivation is involved in the pathogenesis of PAH and this enzyme could be a promising therapeutic target for PAH treatment.

Condensed Abstract

Energy metabolism shift from oxidative phosphorylation towards glycolysis in pulmonary artery smooth muscle cells (PASMCs) is suggested to be involved in their hyperproliferation in pulmonary arterial hypertension (PAH). Here, we demonstrate for the first time the causative link between imbalance of the acetylated/deacetylated state in PASMC associated with weakening of the oxidative phosphorylation machinery and PASMC hyperproliferation, a pulmonary artery hypertension hallmark. As activation of the deacetylase SIRT1 restores mitochondrial biogenesis and normalizes the PASMC phenotype, targeting SIRT1 activity may act as a novel therapy to inhibit PASMC proliferation and thus delay the progression of PAH.

Keywords: pulmonary artery smooth muscle cells; proliferation; oxidative metabolism; mitochondrial biogenesis; sirtuin 1, protein acetylation

Abbreviations

CS – citrate synthase

ERRα - estrogen-related receptor α

FOXO1 - forkhead box protein O1

GLUT1 - glucose transporter 1

HIF-1α - hypoxia-inducible factor-1α

LDH – lactate dehydrogenase

NAMPT - nicotinamide phosphoribosyltransferase

PAH – pulmonary artery hypertension

PASMC - pulmonary artery smooth muscle cells

PDGF - platelet-derived growth factor

PGC-1α - peroxisome proliferator-activated receptor gamma coactivator 1-alpha

SIRT1 – sirtuin 1

SOD2 - superoxide dismutase 2

TFAM - mitochondrial transcription factor A

VDAC - voltage-dependent anion channel

Introduction

Pulmonary arterial hypertension (PAH) is a rare but deadly cardiopulmonary disorder characterized by an extensive remodeling of small- and medium-sized pulmonary arteries, mainly due to the hyperproliferation of pulmonary artery smooth muscle cells (PASMCs). Such vascular remodelling increases pulmonary vascular resistance and pulmonary arterial pressure, ultimately leading to right-sided heart failure and death[1]. The causes that initiate and perpetuate pulmonary vascular cell proliferation in PAH remain unknown, which explains the absence of curative therapies and, thus, the poor prognosis for this disease.

PAH PASMCs share some common features with cancer such as growth dysregulation, resistance to apoptosis, and a metabolic remodeling[2]. Similar to cancer cells, PASMCs display a shift from oxidative phosphorylation towards glycolysis even in the presence of oxygen, condition known as the Warburg effect. This metabolic alteration is sustained by the pathological activation of transcription factors such as c-Myc and the hypoxia-inducible factor-1 α (HIF-1α)[3], as well as the inhibition of the transcription factor forkhead box protein O1 (FOXO1)[4], contributing to PAH PASMC mitochondrial dysfunction. Indeed, PAH PASMC mitochondria present numerous abnormalities (for review, see[5]) including lowered oxidative capacity and altered mitochondrial dynamics leading to mitochondrial fragmentation. The recovery of mitochondrial function via the increase in oxidative capacity[6–8] and/or the restoration of fusion/fission balance[9,10] proved beneficial for the treatment of PAH in animal models, thus appearing as a promising therapeutic approach.

Cellular acetylation/deacetylation balance is an important regulator of energy metabolism including mitochondrial function. Particularly, sirtuin 1 (SIRT1), which is a NAD^+-dependent deacetylase, has been found to augment mitochondrial function via several mechanisms. In various tissues including liver and skeletal muscle, SIRT1 enhances mitochondrial biogenesis and fatty acid oxidation by deacetylating and activating one of the master regulators of mitochondrial biogenesis, PGC-1α (reviewed in[11]). SIRT1 is able to promote mitochondrial gene expression also via a PGC-1α independent pathway. By destabilizing HIF-1α, it prevents HIF-1α-mediated inhibition of c-Myc, activator of the transcription of mitochondrial transcription factor A (TFAM), thus increasing the expression of mitochondrial-encoded respiratory genes[12]. Finally, SIRT1 can improve mitochondrial activity by activating stress signaling pathways via the mitochondrial unfolded protein response and the nuclear translocation and activation of one of FOXO transcription factors as shown in worms[13].

Therefore, one could hypothesize that SIRT1 is affected in PAH and that its activation could have beneficial effects in this disease. However, neither the expression/activity of SIRT1 nor the acetylation/deacetylation balance in PAH pulmonary vessels of patients or in experimental models has been investigated. Of note, another enzyme belonging to this family, sirtuin3, which localizes in the mitochondria to activate metabolic pathways including fatty acid oxidation[14] and oxidative phosphorylation[15,16], is downregulated in human PAH[17]. Importantly, some studies pointed out a potential protective role of SIRT1 in PAH. Indeed, resveratrol, a non-specific SIRT1 activator, has been found to prevent, and even

reverse,[18] monocrotaline-[19] and chronic hypoxia-[20] induced PAH, as well as PAH-associated right ventricle hypertrophy[21]. Furthermore, Ding et al.[22] have recently shown that calorie restriction activates SIRT1 and SIRT1 overexpression can also ameliorate monocrotaline-induced PAH. However, all these studies used non-specific SIRT1 activators, resveratrol and calorie restriction, all of which affect a large range of other targets[23,24]. Moreover, SIRT1-triggered metabolic signaling pathways (which could be involved in resveratrol or calorie restriction beneficial effects on PAH) were not explored.

Here, we investigate the state of SIRT1 signaling pathway in human PAH PASMCs as well as in rat PASMCs stimulated with platelet-derived growth factor (PDGF). We demonstrate that the acetylation/deacetylation balance is shifted towards acetylation in PAH and PDGF-treated PASMCs. We show that SIRT1 is a negative regulator of PASMC growth: its pharmacological inhibition, and specific downregulation enhance human and rat PASMC proliferation. Moreover, we provide evidence for SIRT1 role in vascular remodeling, since its genetic deletion aggravates chronic hypoxia-induced pulmonary artery muscularization in mice. We then prove that SIRT1 can have beneficial effect in PAH treatment by using the SIRT1 specific activator Stac-3, which completely prevents PDGF-induced proliferation and, importantly, abolishes almost completely the proliferation of PASMCs from PAH patients without effect on the cell mortality. Finally, we show that SIRT1 activation is associated with the increase in the expression of genes implicated in mitochondrial function and the augmentation of mitochondrial biogenesis, thus providing a mechanistic explanation for the role of acetylation/deacetylation balance.

Material and Methods

Rat and human PASMCs

Primary culture of rat PASMCs were derived from 13 250-300 g male Wistar rats. After anaesthesia via intraperitoneal injection of sodium pentobarbital (100 mg/kg), the trachea, heart and lungs were rapidly removed, and the pulmonary artery isolated and deprived of residual adventitial tissue using dissection forceps and tweezers. Pulmonary artery was then cut in small pieces and incubated in 1% antibiotic/antimycotic (a/a) Dulbecco's modified eagle medium (DMEM) containing 150 U/mL type I collagenase and 0.125 mg/mL elastase at 37°C for 90 minutes under shaking. Tissue lysate was then filtered through a 70 µm cell strainer. Cells were collected and cultivated in 15% fetal bovine serum (FBS) and 1% a/a DMEM at 37°C in a 95% air-5% CO2 atmosphere till subconfluence. Medium was changed every other day. Culture material was previously coated with 50 µg/mL collagene I. Experiments were performed between passages 2 and 6. All animal care and experimental procedures conformed to the European Community guiding principles in the care and use of animals (Directive 2010/63/EU of the European Parliament) and authorizations to perform animal experiments according to this decree were obtained from the French Ministry of Agriculture, Fisheries and Food (No. D-92-283, 13 December 2012).

Human PASMCs were prepared from pulmonary artery explants (5-10 mm of diameter) obtained during lung transplantation from 5 patients with idiopathic PAH and during lobectomy or pneumonectomy for localized lung cancer from 7 control (CTL) subjects (Table 1). In control subjects, pulmonary arteries explants were isolated at a distance from tumor areas. Transthoracic echocardiography was

performed preoperatively in the control subjects to rule out pulmonary hypertension. Patients studied were part of the French Network on Pulmonary Hypertension, a program approved by our institutional Ethics Committee, and had given written informed consent (Protocol N8CO-08- 003, ID RCB: 2008-A00485-50, approved on June 18, 2008). The principles of the Declaration of Helsinki were followed. Human PASMCs were cultivated in DMEM containing glucose (4.5 g/L), FBS (15%), L-glutamine (2 mmol/L), HEPES (20 mmol/L), epidermal growth factor (EGF) (10 U/mL), insulin-transferrin-selenium (ITS) 1X, normocin (0.1 mg/mL), 1% a/a, and used until passage 6.

Treatments of rat and human PASMCs

After 24-hour incubation in 0.5% FBS and 1% a/a supplemented medium, PASMCs were pre-incubated for 2 hours with one of the following compounds diluted in the same medium: 10µmol/L Stac-3 (Santa Cruz, Heidelberg, Germany, sc-222315), 5 µmol/L sirtinol (Santa Cruz, Heidelberg, Germany, sc-205976) and 1 µmol/L SRT1720 (APExBIO, Houston, TX, A4180). Control cells were treated with vehicle (DMSO). Rat PASMC proliferation was then induced with 10 ng/mL PDGF for 24 hours. Since PAH PASMCs maintain their hyperproliferative phenotype in culture, no compound was used to stimulate their growth.

Evaluation of PASMC proliferation and death

PASMC proliferation was measured via four different approaches. BrdU incorporation was evaluated using a kit (Millipore, Molsheim, France), following the manufacturer instructions. WST-1 (Sima Aldrich, Saint Quentin Fallavier, France) cleavage was measured by a spectrophotometer. Cell counting was performed using a Malassez haemocytometer. The protein amount of proliferating cell nuclear antigen (PCNA) was detected via Western blotting (WB).

For measuring PASMC death, cells were labeled with 0.1 µg/mL fluorescein diacetate (FDA), and FDA negative cells were detected by flow cytometry (FC500, Beckman Coulter, Villepinte, France). To analyze late apoptosis/necrosis, cells were also labeled with 10 µg/mL propidium iodide (PI). Only late apoptotic/necrotic cells, which have lost their membrane integrity, can be labeled by this nucleic acid intercalating fluorescent agent.

For each sample, at least 7 500 cells were analyzed. Cell aggregates and debris were excluded from analysis.

PASMC transient transfection

Reverse short interference RNA transfection was performed to downregulate SIRT1 in rat and human PASMCs. Cells were seeded in a transfection medium (Santa Cruz) containing transfection reagent (Santa Cruz) and a mix of three short interfering RNA specifically directed against SIRT1 (siSIRT1, Santa Cruz) or having no known target (control siRNA-A, Santa Cruz). 24 hours after the transfection, cells were cultivated for additional 24 hours with 0.5% FBS containing medium, then treated. Transfection rate, evaluated by flow cytometry using a FITC-coupled siRNA (Santa Cruz), was about 60%. Transfection efficiency was confirmed by SIRT1 protein level.

Immunohistochemistry

7-µm thicked slices were cut and stained with α smooth muscle actin (αSMA) (Sigma, F3777, 1:200), Von Willebrand endothelial factor (VWF) (DAKO, A0082, 1:600) and 4 µmol/L Hoechst for nuclear staining. For each mouse, 100 small vessels (with a

diameter <50µm) were examined by a blinded observer. Each vessel was categorized as non muscular (vessels without smooth muscle), partially muscular (vessels with smooth muscle layer in only part of their wall) or totally muscular (smooth muscle is identifiable in the entire vessel circumference).

Immunoprecipitation

The lysates of PASMCs, including 500 µg protein, were precleaned with protein A magnetic beads (Millipore) at 4°C for 1 hour, and then supernatants were collected. The lysates were incubated with anti-acetylated lysine antibody (Cell Signalling, 9681, 1:20) or with anti-mouse IgG antibodies (Santa Cruz, sc-2025, 1:20) at 4°C overnight. Immune complexes were collected then resuspended in denaturing lysis buffer and heated at 70°C for 10 minutes. The immunoprecipitated proteins were subjected to Western blot analysis for PGC-1α detection.

Immunoblot

30 to 50 µg of protein extract were loaded onto 8-15% polyacrylamide gel, and then transferred onto a PVDF membrane (Immobilon, Millipore).
Primary antibody (see supplementary Table S1) incubation was performed either overnight at 4°C or for 2 hours at room temperature. The incubation of peroxydase-coupled secondary antibody was realized for 1 hour at room temperature. Proteins were visualized using Luminata Crescendo or Forte (Millipore) peroxydase substrates using a CCD camera (ChemiDoc XRS+Bio-rad). Band density was quantified using Quantity One software (BioRad) and normalized to a housekeeping protein (β actin for human PASMCs or vinculin for rat PASMCs).

Quantitative RT-PCR

Total RNAs were extracted from cells using TRIzol (Molecular Research Center). Briefly, chloroform was added to TRIzol, samples were centrifuged at 10000 g for 15 minutes at 4°C, and three phases were thus obtained: a protein containing phenol-chloroform fraction, a DNA containing interphase and a RNA containing aqueous phase.
The addition of isopropanol to the aqueous phase allowed RNA precipitation. Reverse transcription was performed from 1 µg RNA in 20µl using BioRad complementary DNA (cDNA) synthesis kit, following manufacturer instructions. Negative controls without reverse transcriptase were performed to verify the absence of genomic DNA in the samples.
Gene expression was evaluated using a quantitative PCR system (BioRad) with SYBR-Green dye. PCR reaction was realized on 5 µl of the reverse transcription reaction product diluted by 20. Reaction mix contained 0.5 µmol/L sense and anti-sens primers (see supplementary Table S2). To confirm the absence of exogenous contaminations, a negative control without sample was realized. For each gene, a calibration curve was obtained analyzing cDNA series dilutions, and was used to calculate sample concentration and determine amplification efficiency. TBP (TATA-Binding Protein), RPL32 (Ribosomal Protein Large 32), RPLP2 (Ribosomal Protein Large P2) and 14-3-3 zeta/delta protein (YWHAZ) were used as reference genes for rat PASMCs to obtain a normalization factor calculated by GeNorm software. For human PASMCs, RPL32, TBP, RPLP0 (Ribosomal Protein Large P0) and RPL4 (Ribosomal Protein Large 4) were used as reference genes.

In vivo study

Inducible SIRT1 KO mice were kindly provided by Dr. D.A.Sinclair (Harvard Medical School, Boston, MA)1. 3-month old female mice (C57BL/6J carrying both the UBC-Cre-ERT2 and the SIRT1floxΔE4/floxΔE4 alleles) were subjected to an injection of tamoxifene (30mg/kg) per day for four consecutive days to induce SIRT1 deletion. WT mice were injected with the same concentration of vehicle (peanut oil). After three weeks, mice were exposed to chronic hypoxia (10% O2) in a ventilated chamber (Biospherix, New York, NY). A mixture of room air and nitrogen was flushed in the chamber to maintain the hypoxic environment. Normoxic mice were kept in the same room, with the same light/dark cycle. After three weeks of hypoxia exposure, mice were anesthetized with 4%, 3 L/min isoflurane. After skin incision of the sternum, direct transthoracic insertion of a catheter into the right ventricle was performed, and right ventricle pressure was measured via PowerLab 4/35 software. The thorax was opened, mice were then euthanatized via exsanguination from the aorta, and the lungs and heart rapidly removed. The right ventricle (RV) was dissected from the left ventricle plus septum (LV+S), and then the samples were weighted for determining the Fulton's index (RV/(LV+S)). Right lungs were injected with a solution 1:1 of OCT (optimal cutting temperature) and physiological serum, and then frozen for subsequent immunohistochemical analysis, and left lungs were frozen for WB.

Mitochondrial network analysis

Cells were incubated for 15 minutes at 37°C with 500 nmol/L MitoTracker Orange MTO for mitochondrial staining. Cells were then fixed with 4% PFA for 10 min at 37°C, auto-fluorescence was quenched via 5-minute incubation with 50 mmol/L NH_4Cl and were mounted using mowiol mounting medium.
3D confocal images were acquired collecting a Z-series stack with 63x objective by an inverted Laser Scanning Microscope (Zeiss LSM 510). MTO was excited by 543 nm helium neon laser. 3D images were deconvoluted using AutoDeblur AutoVisualize software (MediaCybernetics) to increase confocal system resolution, and then analyzed using Imaris software (Bitplane Company) to provide information on mitochondrial volume.

Statistical analysis

The data are presented as mean±SEM. For cell culture experiments, n means number of batches each being derived from one patient/animal.
For Stac-3 and SRT1720 treatment of rat PASMC, differences were determined using one-way analysis of variance followed by Newman-Keuls post-hoc test. For short interference experiments, sirtinol treatment and in vivo study, differences were evaluated using a two-way analysis of variance followed by Newman-Keuls post-hoc test. Human CTL and PAH PASMCs were compared using Mann-Whitney U test. Differences were considered as significant when p-value <0.05.

Results

Metabolic Profile in Human PAH PASMCs

In PASMCs from idiopathic PAH patients (PAH PASMCs), mitochondrial mass was decreased compared with control PASMCs (CTL PASMCs) as evidenced by reduced mitochondrial voltage-dependent anion channel (VDAC) and citrate synthase (CS) protein content (Fig.1A). Consistently, the protein level of mitochondrial biogenesis master regulator PGC-1α was reduced in PAH PASMCs, and this was associated with a downregulation of its targets including the transcription factor peroxisome proliferator-activated receptor α (PPARα) and the estrogen-related receptor α (ERRα) as well as the antioxidant enzyme superoxide dismutase 2 (SOD2) (Fig.1B). In parallel, the glucose transporter 1 (GLUT1) and lactate dehydrogenase (LDH) protein levels were increased (Fig.1C). Thus, these results suggest an energy metabolism shift from mitochondrial oxidative phosphorylation towards glycolytic pathway in human PAH.

Acetylation/deacetylation balance in PAH PASMCs and PDGF-treated rat PASMCs

Deacetylation of PGC-1α is one of main regulators of its activity, therefore we hypothesized that a downregulation of mitochondrial biogenesis cascade in PAH PASMCs controlled by PGC-1α could be linked to altered acetylation/deacetylation balance. The deacetylase SIRT1 gene expression (Fig.2A) and protein content of SIRT1 were unaffected in PAH PASMCs, as well as the protein content of nicotinamide phosphoribosyltransferase (NAMPT) (Fig.2B), an enzyme that produces the SIRT1 cofactor NAD^+ [25] . However, the balance between the acetylated and total forms of the SIRT1 targets PGC-1α and histone H1 (Fig.2C) was shifted towards higher acetylation in PAH PASMCs. Thus, this shift towards acetylation suggests that the SIRT1 signaling pathway is impaired in PAH PASMCs. Qualitatively similar results were obtained in rat PASMCs, where PDGF-induced proliferation (Fig.2D) was associated with increased content of the acetylated forms of PGC-1α and histone H1 as well as that of FOXO1, another SIRT1 target[26] (Fig.2E) .

Effect of SIRT1 downregulation or inhibition on human and rat PASMC proliferation

Next, we investigated whether altered acetylation/deacetylation balance could play a causative role in PASMC hyperproliferation. We downregulated SIRT1 expression by 85% via siRNA in control human PASMCs (Fig.3A). The decline in SIRT1 protein level boosted CTL PASMC proliferation, as shown by the 50% increase in the incorporation of the thymidine analog BrdU by replicating cells (Fig.3A). In order to confirm this finding, we silenced SIRT1 also in rat PASMCs. Again, the reduced level of SIRT1 (by almost 70%, Fig.3B) enhanced PDGF-induced proliferation, as evidenced by the increase in cell number quantified by WST-1 cleavage by viable cells and BrdU incorporation (Fig.3B). We further corroborated these observations by showing a facilitation of PDGF-induced proliferation also via SIRT1 pharmacological inhibition with sirtinol (Fig.3C). Thus, these results indicate that SIRT1 downregulation could be a causative factor for PASMC hyperproliferation.

Impact of SIRT1 genetic deletion on pulmonary vascular remodeling

We then investigated the potential role of SIRT1 downregulation in vascular remodeling induced by chronic hypoxia exposure known to trigger SMC proliferation. Thus, SIRT1 inducible knock out (SIRT1 KO) mice and their wild type (WT) littermates were exposed to either chronic hypoxia or normoxia for three weeks. As represented in Fig.4A, the deletion of SIRT1 exon 4 which encodes the catalytic domain led to the production of a non-functional protein. SIRT1 wild-type protein was significantly reduced in SIRT1 KO lungs both in normoxia and hypoxia, respectively by 67% and 80%. In control lungs, chronic hypoxia exposure induced a slight increase in PGC-1α protein level, which was completely absent in SIRT1 KO lungs. Interestingly, hypoxia-induced increase of the transcription factor HIF-1α was less pronounced in SIRT1 KO compared to wild-type (WT) mice, whereas GLUT1 induction after chronic hypoxia was higher in SIRT1 deficient mice.
A deeper vascular remodeling, with an increase in the percentage of completely muscular pulmonary arteries, paralleled by a decrease in the percentage of non-muscular arteries, was observed in mutant lungs. The percentage of partially muscular vessels was also slightly increased in KO compared to WT mice lungs (Fig.4B). This was associated with an exacerbated increase in the right ventricle pressure and hypertrophy (Fig.4C).Thus, the inactivation of SIRT1 aggravates vascular and cardiac remodeling *in vivo*.

Inhibition of PASMC hyperproliferation via SIRT1 pharmacological activation

To test whether correction of the acetylation/deacetylation balance could have beneficial effect on PASMC hyperproliferation, we investigated the effects of the pharmacological activator of SIRT1 Stac-3. As expected, Stac-3 significantly decreased the content of acetylated SIRT1 targets histone H1 and FOXO1 in rat PASMCs as well as PGC-1α (Fig.5A). Since SIRT1 seemed to be also involved in the expression of NAMPT[27,28], the rate-limiting enzyme in the NAD^+ biosynthetic pathway, we studied this expression and found that Stac-3 considerable increased NAMPT mRNA level (supplemental Fig.I), thus favoring the synthesis of the SIRT1 cofactor.
Next, we studied the effect of Stac-3 on PDGF-induced proliferation in rat PASMCs. This treatment completely abolished PDGF proliferative effect (Fig.5B). Moreover, the protein level of the proliferation marker PCNA was reduced when Stac-3 was added to PDGF-treated PASMCs (Fig.5B). To further verify this observation, we used another SIRT1 activator, SRT1720. This compound also stunted PASMC proliferation but to a lesser extent (Fig.5C). Importantly, the anti-proliferative effect of Stac-3 was not associated with an increase in cell death. Indeed, Stac-3 increased neither the percentage of cells unable to cleave the viability marker FDA nor the percentage of propidium iodide permeable necrotic cells (Fig.5D).
Given the inhibitory effect of SIRT1 activation on rat PASMC proliferation, we tested Stac-3 in PAH PASMCs. The proliferation of these cells was almost completely abolished, with a decrease by more than 50% of WST-1 cleavage, a reduction of BrdU incorporation by 80% and the diminution of the protein content of the proliferation marker PCNA by almost 50% (Fig.5E).

The state of PGC-1α downstream cascade and mitochondrial biogenesis upon SIRT1 activation

To provide mechanistic insights into the pathways potentially implicated in Stac-3 effect on PASMC proliferation, mRNA and protein levels of several actors of

mitochondrial bioenergetics were analyzed. Stac-3-mediated SIRT1 activation increased PAH PASMC mitochondrial mass, as evidenced by the elevation of VDAC and CS protein level (Fig.6A). This augmentation can be explained by activation of mitochondrial biogenesis as Stac-3 increased the expression of PGC-1α molecular partners PPARα and ERRα as well as the expression of the antioxidant enzyme SOD2, known to be regulated by PGC-1α[29] (Fig.6B). Similar results were obtained in rat PASMCs, where Stac-3 also promoted mitochondrial biogenesis, as indicated by the increase of VDAC and CS protein level, as well as of TFAM (Fig.6C). In rat cells, Stac-3 also activated the expression of PGC-1α partners (PPARα, ERRα and NRF2), and the elements of PGC-1α-triggered cascade (TFAM, antioxidant enzyme glutathione peroxidase 1, and mitochondrial deacetylase sirtuin 3) (Fig.6D). Therefore, SIRT1 activation is clearly associated with the concerted upregulation of mitochondrial biogenesis pathway.

Effects of SIRT1 activation on mitochondrial morphology

Since mitochondrial fragmentation can favor the hyperproliferation, we also studied SIRT1 effect on mitochondrial morphology. Stimulation with PDGF induced mitochondrial fragmentation, which was abolished by Stac-3 treatment (Fig.7A and B). SIRT1 activation thus normalizes mitochondrial morphology by inhibiting hyperproliferation-associated excessive fragmentation.

Discussion

The present study has highlighted a potential role of the deacetylase SIRT1, an important modulator of cell metabolism, in PASMC hyperproliferation, SIRT1 is a powerful negative regulator of rat and human PASMC proliferation and a deficiency in SIRT1 can be a factor favoring vascular remodeling. Conversely, SIRT1 activation could be considered as an effective tool to inhibit PASMC proliferation.

PAH PASMCs exhibited reduced expression of VDAC and CS, mitochondrial mass markers, confirming the rarefaction of the mitochondrial network observed in patients' cells in an earlier study[3]. This was associated with a negative regulation of mitochondrial biogenesis, as indicated by the decreased protein level of PGC-1α, also shown by Ryan et al.[10], as well as with the reduced expression of its targets, the transcription factors PPARα and ERRα and the antioxidant enzyme SOD2. The partial loss of mitochondrial mass by PAH PASMCs was counterbalanced by a considerable increase in GLUT1 expression, which agrees with the increase in glycolytic flux determined by the uptake of glucose analogue FDG by PAH patients' lungs[30]. The LDH expression was also increased, thus favoring the uncoupling of glycolysis from glucose oxidation. Such a remodeling could contribute to the increased plasma lactate levels found in Chuvash PAH[31], as well as in idiopathic PAH patients[32].

The observed loss of mitochondrial mass in PAH PASMCs suggests a negative regulation of mitochondrial biogenesis probably at least in part due to downregulation of the PGC-1α-regulated cascade. Indeed, protein content of this master regulator of mitochondrial biogenesis is lowered. Besides, its activity is known to be modulated by post-translational modifications, such as the acetylation/deacetylation balance. Regardless of the activity of cell acetylases and deacetylases, the domination of acetylated forms of various cell targets (histone H1, FOXO1, PGC-1α) in PAH and PDGF-stimulated rat PASMCs shows a clear shift of the balance towards acetylation. The causal link between weakened deacetylation activity and PASMC proliferation has been provided by experiments using SIRT1 silencing or pharmacological inhibition by sirtinol. Indeed, both interventions increased rat and human PASMC proliferation, providing the first evidence of pathogenic role of acetylation in PASMC hyperproliferation, which could be overcome by SIRT1 activity.

The positive anti-proliferative role of SIRT1 was further confirmed in the experiments where SIRT1 deletion in mice significantly aggravated vascular remodeling induced by chronic hypoxia exposure. This effect was accompanied by an increase in right ventricle pressure and hypertrophy. Interestingly, SIRT1 deficiency abolished hypoxia-induced increase in PGC-1α protein level seen in WT lungs and this could attenuate PGC-1α–controlled pathways including mitochondrial biogenesis. We and others[33] have shown that hypoxia increases SIRT1 expression which is able to regulate PGC-1α transcription[34]. In SIRT1 KO lungs, hypoxia-mediated increase in SIRT1 expression was blocked and this could abolish the augmentation of PGC-1α expression. A marked rise in GLUT1 expression in SIRT1 KO lungs argues that under hypoxic conditions, SIRT1 deficiency induces an imbalance in favor of glycolysis at the expense of oxidative phosphorylation.

Recently it has been demonstrated that SIRT1 can maintain mitochondrial biogenesis also via a PGC-1α-independent pathway[12]. SIRT1 stabilizes the ubiquitin ligase Von Hippel-Lindau (VHL), which recognizes HIF-1α hydroxylated prolines, thus leading to the degradation of this transcription factor. Since HIF-1α inhibits c-myc,

transcription factor activator of TFAM expression, SIRT1-mediated HIF-1α downregulation positively modulates TFAM and, consequently, mitochondrial gene expression[12]. However, in our experiments, HIF-1α protein level was unaltered by SIRT1 deficiency under normoxia. In chronic hypoxia, SIRT1 KO lungs show a reduced HIF-1α response. Therefore, PAH aggravation in SIRT1 KO mice seems to be independent of this transcription factor.

It has been proposed that the stimulation of mitochondrial metabolism could be a promising therapeutic approach to proliferative disorders such as cancer[35]. Reversing the metabolic shift from oxidative metabolism to glycolysis has proved to be efficient to treat PAH in animal models, and is currently the subject of clinical trials[5]. Here, we show that the pharmacological activation of SIRT1 by Stac-3 leads to a strong inhibition of PAH PASMCs proliferation without effect on cell viability. An increase in the expression of transcription factors involved in mitochondrial biogenesis was observed, with a subsequent increase in mitochondrial mass. These effects of Stac-3 seem to be a consequence of direct SIRT1 activation because Stac-3 has no effect on mitochondrial mass in cells reconstituted with activation-defective SIRT1[36]. More detailed investigation carried out on rat PASMCs has shown that Stac-3 increases the expression of different factors maintaining mitochondrial biogenesis (PPARα, ERRα, NRF2, TFAM). Moreover, SIRT1 activation prevents PDGF-induced mitochondrial fragmentation. Interestingly, a recent study has demonstrated that mitochondrial fission is essential for PAH PASMC proliferation; its inhibition causes cell cycle arrest and ameliorates PAH experimental models[9]. In parallel, mitofusin 2, a protein involved in mitochondrial fusion, is downregulated in PAH PASMCs, and the restoration of its expression inhibits PAH PASMC hyperproliferation[10]. Thus, prevention of proliferation-induced mitochondrial fission by Stac-3 could also contribute to inhibition of PASMC proliferation. Finally, Stac-3 treatment leads to the increase of SOD2 expression, whose downregulation has been shown to contribute to PAH PASMC hyperproliferation. Indeed, SOD2 promoter and enhancer were found to be hypermethylated leading to a decrease in its expression[37]. This in turn led to a decrease in H_2O_2 production, thus allowing HIF-1α stabilization and K_V potassium channel inhibition, both pro-proliferative events[37]. The decrease in SOD2 expression could thus be due to a combination of epigenetic inhibition and downregulation of the co-activator controlling its transcription. Therefore, its induction upon SIRT1 activation could be partly responsible for Stac-3 anti-proliferative effects.

Such a concerted upregulation of various factors controlled by PGC-1α supports the hypothesis that the metabolic remodeling associated with the hyperproliferation inhibition induced by Stac-3 involves PGC-1α activation via deacetylation. SIRT1-mediated deacetylation of other targets may also play a role. Indeed, SIRT1 catalyses the deacetylation of FOXO1 thus potentiating its transcriptional activity[38]. Yet, PASMC FOXO1 is a critical integrator of multiple signaling pathways driving PAH, and reconstitution of FOXO1 activity is able to restore the physiologically quiescent PASMC phenotype.[4] Regardless of the relative contribution of PGC-1α or FOXO1 deacetylation to the inhibition of PASMC hyperproliferation, the activation of SIRT1 leads to the same endpoint.

In summary, our results demonstrate the causative link between imbalance of the acetylated/deacetylated state in PASMC associated with weakening of the oxidative phosphorylation machinery and PASMC hyperproliferation, a PAH hallmark. As activation of the deacetylase SIRT1 restores mitochondrial biogenesis and

normalizes the PASMC phenotype, targeting SIRT1 activity is potentially a novel therapy to inhibit PASMC proliferation and thus delay the progression of PAH. Such a new strategy for PAH treatment, which reinforces cell oxidative capacities via correction of the acetylation/deacetylation balance may also be beneficial for the failing right ventricle overloaded in PAH. Given that SIRT1 upregulation seems to be also beneficial for the systemic arteries and for the heart (see[39,40] and references therein), effects of specific SIRT1 activation on the entire cardiovascular system should also be evaluated.

Acknowledgments
We thank Dr. V. Nicolas (Imaging facility of IFR141), Dr. V. Domergue (Animal facility of IFR141) and Dr. C. Deloménie (Transcriptomic platform of IFR141) for technical help. The authors would also like to thank Dr.R. Fischmeister, Dr. A.-M. Gomez, Dr. S. Cohen-Kaminsky for continuous support and A. Truong for his kind proofreading.

References

1 Humbert M, Lau EMT, Montani D, Jaïs X, Sitbon O, Simonneau G. Advances in Therapeutic Interventions for Patients With Pulmonary Arterial Hypertension. *Circulation* 2014; 130:2189–2208.

2 Paulin R, Michelakis ED. The metabolic theory of pulmonary arterial hypertension. *Circ Res* 2014; 115:148–164.

3 Bonnet S, Michelakis ED, Porter CJ, Andrade-Navarro MA, Thébaud B, Bonnet S, *et al.* An abnormal mitochondrial-hypoxia inducible factor-1alpha-Kv channel pathway disrupts oxygen sensing and triggers pulmonary arterial hypertension in fawn hooded rats: similarities to human pulmonary arterial hypertension. *Circulation* 2006; 113:2630–2641.

4 Savai R, Al-Tamari HM, Sedding D, Kojonazarov B, Muecke C, Teske R, *et al.* Pro-proliferative and inflammatory signaling converge on FoxO1 transcription factor in pulmonary hypertension. *Nat Med* 2014; 20:1289–1300.

5 Ryan JJ, Archer SL. Emerging Concepts in the Molecular Basis of Pulmonary Arterial Hypertension Part I: Metabolic Plasticity and Mitochondrial Dynamics in the Pulmonary Circulation and Right Ventricle in Pulmonary Arterial Hypertension. *Circulation* 2015; 131:1691–1702.

6 McMurtry MS, Bonnet S, Wu X, Dyck JRB, Haromy A, Hashimoto K, *et al.* Dichloroacetate prevents and reverses pulmonary hypertension by inducing pulmonary artery smooth muscle cell apoptosis. *Circ Res* 2004; 95:830–840.

7 Michelakis ED, McMurtry MS, Wu X-C, Dyck JRB, Moudgil R, Hopkins TA, *et al.* Dichloroacetate, a metabolic modulator, prevents and reverses chronic hypoxic pulmonary hypertension in rats: role of increased expression and activity of voltage-gated potassium channels. *Circulation* 2002; 105:244–250.

8 Sutendra G, Bonnet S, Rochefort G, Haromy A, Folmes KD, Lopaschuk GD, *et al.* Fatty Acid Oxidation and Malonyl-CoA Decarboxylase in the Vascular Remodeling of Pulmonary Hypertension. *Sci Transl Med* 2010; 2:44ra58-44ra58.

9 Marsboom G, Toth PT, Ryan JJ, Hong Z, Wu X, Fang Y-H, *et al.* Dynamin-Related Protein 1–Mediated Mitochondrial Mitotic Fission Permits Hyperproliferation of Vascular Smooth Muscle Cells and Offers a Novel Therapeutic Target in Pulmonary Hypertension. *Circ Res* 2012; 110:1484–1497.

10 Ryan JJ, Marsboom G, Fang Y-H, Toth PT, Morrow E, Luo N, *et al.* PGC1α-mediated mitofusin-2 deficiency in female rats and humans with pulmonary arterial hypertension. *Am J Respir Crit Care Med* 2013; 187:865–878.

11 Houtkooper RH, Pirinen E, Auwerx J. Sirtuins as regulators of metabolism and healthspan. *Nat Rev Mol Cell Biol* 2012; 13:225–238.

12 Gomes AP, Price NL, Ling AJY, Moslehi JJ, Montgomery MK, Rajman L, *et al.* Declining NAD(+) induces a pseudohypoxic state disrupting nuclear-mitochondrial communication during aging. *Cell* 2013; 155:1624–1638.

13 Mouchiroud L, Houtkooper RH, Moullan N, Katsyuba E, Ryu D, Cantó C, *et al.* The NAD+/Sirtuin Pathway Modulates Longevity through Activation of Mitochondrial UPR and FOXO Signaling. *Cell* 2013; 154:430–441.

14 Hirschey MD, Shimazu T, Goetzman E, Jing E, Schwer B, Lombard DB, *et al.* SIRT3 regulates fatty acid oxidation via reversible enzyme deacetylation. *Nature* 2010; 464:121–125.

15 Ahn B-H, Kim H-S, Song S, Lee IH, Liu J, Vassilopoulos A, *et al.* A role for the mitochondrial deacetylase Sirt3 in regulating energy homeostasis. *Proc Natl Acad Sci U S A* 2008; 105:14447–14452.

16 Cimen H, Han M-J, Yang Y, Tong Q, Koc H, Koc EC. Regulation of Succinate Dehydrogenase Activity by SIRT3 in Mammalian Mitochondria. *Biochemistry (Mosc)* 2010; 49:304–311.

17 Paulin R, Dromparis P, Sutendra G, Gurtu V, Zervopoulos S, Bowers L, *et al.* Sirtuin 3 Deficiency Is Associated with Inhibited Mitochondrial Function and Pulmonary Arterial Hypertension in Rodents and Humans. *Cell Metab* doi:10.1016/j.cmet.2014.08.011

18 Paffett ML, Lucas SN, Campen MJ. Resveratrol reverses monocrotaline-induced pulmonary vascular and cardiac dysfunction: A potential role for atrogin-1 in smooth muscle. *Vascul Pharmacol* 2012; 56:64–73.

19 Csiszar A, Labinskyy N, Olson S, Pinto JT, Gupte S, Wu JM, *et al.* Resveratrol prevents monocrotaline-induced pulmonary hypertension in rats. *Hypertension* 2009; 54:668–675.

20 Chen B, Xue J, Meng X, Slutzky JL, Calvert AE, Chicoine LG. Resveratrol prevents hypoxia-induced arginase II expression and proliferation of human pulmonary artery smooth muscle cells via Akt-dependent signaling. *Am J Physiol Lung Cell Mol Physiol* 2014; 307:L317-325.

21 Yang D-L, Zhang H-G, Xu Y-L, Gao Y-H, Yang X-J, Hao X-Q, *et al.* Resveratrol inhibits right ventricular hypertrophy induced by monocrotaline in rats. *Clin Exp Pharmacol Physiol* 2010; 37:150–155.

22 Ding M, Lei J, Qu Y, Zhang H, Xin W, Ma F, *et al.* Calorie Restriction Attenuates Monocrotaline-induced Pulmonary Arterial Hypertension in Rats. *J Cardiovasc Pharmacol* 2015; 65:562–570.

23 Bitterman JL, Chung JH. Metabolic effects of resveratrol: addressing the controversies. *Cell Mol Life Sci CMLS* 2015; 72:1473–1488.

24 Testa G, Biasi F, Poli G, Chiarpotto E. Calorie restriction and dietary restriction mimetics: a strategy for improving healthy aging and longevity. *Curr Pharm Des* 2014; 20:2950–2977.

25 Revollo JR, Grimm AA, Imai S. The NAD biosynthesis pathway mediated by nicotinamide phosphoribosyltransferase regulates Sir2 activity in mammalian cells. *J Biol Chem* 2004; 279:50754–50763.

26 Motta MC, Divecha N, Lemieux M, Kamel C, Chen D, Gu W, *et al.* Mammalian SIRT1 Represses Forkhead Transcription Factors. *Cell* 2004; 116:551–563.

27 Nakahata Y, Sahar S, Astarita G, Kaluzova M, Sassone-Corsi P. Circadian control of the NAD+ salvage pathway by CLOCK-SIRT1. *Science* 2009; 324:654–657.

28 Bellet MM, Nakahata Y, Boudjelal M, Watts E, Mossakowska DE, Edwards KA, *et al.* Pharmacological modulation of circadian rhythms by synthetic activators of the deacetylase SIRT1. *Proc Natl Acad Sci U S A* 2013; 110:3333–3338.

29 Valle I, Alvarez-Barrientos A, Arza E, Lamas S, Monsalve M. PGC-1alpha regulates the mitochondrial antioxidant defense system in vascular endothelial cells. *Cardiovasc Res* 2005; 66:562–573.

30 Zhao L, Ashek A, Wang L, Fang W, Dabral S, Dubois O, *et al.* Heterogeneity in lung (18)FDG uptake in pulmonary arterial hypertension: potential of dynamic (18)FDG positron emission tomography with kinetic analysis as a bridging biomarker for pulmonary vascular remodeling targeted treatments. *Circulation* 2013; 128:1214–1224.

31 Formenti F, Constantin-Teodosiu D, Emmanuel Y, Cheeseman J, Dorrington KL, Edwards LM, *et al.* Regulation of human metabolism by hypoxia-inducible factor. *Proc Natl Acad Sci* 2010; 107:12722–12727.

32 HU E-C, HE J-G, LIU Z-H, NI X-H, ZHENG Y-G, GU Q, *et al.* High levels of serum lactate dehydrogenase correlate with the severity and mortality of idiopathic pulmonary arterial hypertension. *Exp Ther Med* 2015; 9:2109–2113.

33 Chen R, Dioum EM, Hogg RT, Gerard RD, Garcia JA. Hypoxia Increases Sirtuin 1 Expression in a Hypoxia-inducible Factor-dependent Manner. *J Biol Chem* 2011; 286:13869–13878.

34 Amat R, Planavila A, Chen SL, Iglesias R, Giralt M, Villarroya F. SIRT1 controls the transcription of the peroxisome proliferator-activated receptor-gamma Co-activator-1alpha (PGC-1alpha) gene in skeletal muscle through the PGC-1alpha autoregulatory loop and interaction with MyoD. *J Biol Chem* 2009; 284:21872–21880.

35 Galluzzi L, Kepp O, Vander Heiden MG, Kroemer G. Metabolic targets for cancer therapy. *Nat Rev Drug Discov* 2013; 12:829–846.

36 Hubbard BP, Gomes AP, Dai H, Li J, Case AW, Considine T, *et al.* Evidence for a Common Mechanism of SIRT1 Regulation by Allosteric Activators. *Science* 2013; 339:1216–1219.

37 Archer SL, Marsboom G, Kim GH, Zhang HJ, Toth PT, Svensson EC, *et al.* Epigenetic attenuation of mitochondrial superoxide dismutase 2 in pulmonary arterial hypertension: a basis for excessive cell proliferation and a new therapeutic target. *Circulation* 2010; 121:2661–2671.

38 Daitoku H, Hatta M, Matsuzaki H, Aratani S, Ohshima T, Miyagishi M, *et al.* Silent information regulator 2 potentiates Foxo1-mediated transcription through its deacetylase activity. *Proc Natl Acad Sci U S A* 2004; 101:10042–10047.

39 Tanno M, Kuno A, Horio Y, Miura T. Emerging beneficial roles of sirtuins in heart failure. *Basic Res Cardiol* 2012; 107:273.

40 Liao Y-C, Wang Y-S, Guo Y-C, Lin W-L, Chang M-H, Juo S-HH. Let-7g improves multiple endothelial functions through targeting transforming growth factor-beta and SIRT-1 signaling. J Am Coll Cardiol 2014; 63:1685–1694.1

Table 1: Characteristics of PAH and control patients.

Patient	Age yr	Gender	NYHA class	mPAP, mm Hg	Cardiac index, $L.min^{-1}.m^{-2}$	Specific medication
PAH	41	F	4	50	3.4	PDE5i, ERA
PAH	44	F	4	50	N/C	
PAH	35	F	3	53	2.15	PDE5i, ERA, PC
PAH	26	F	4	94	1.7	ERA, PC
PAH	44	M	4	N/A	N/C	LTRA
CTR	43	F				
CTR	56	F				
CTR	56	M				
CTR	64	M				
CTR	65	M				
CTR	78	M				
CTR	61	F				

PDE5i: phosphodiesterase class 5 inhibitors, ERA: endothelin receptor antagonists; PC: prostacyclin; LTRA: leukotriene receptor antagonists; N/C: non-communicated

Captions

Figure 1. PAH PASMC metabolic profile is shifted from oxidative phopshorylation towards glycolysis.

(A) PAH PASMCs display a decreased protein level of VDAC and CS, two markers of mitochondrial mass (n=4). (B) The expression of the transcriptional co-activator PGC-1α is reduced in PAH PASMCs, characterized also by a decrease in the mRNA content of PPARα, ERRα and SOD2 (n=4). (C) The expression of glucose transporter GLUT1 and LDH is increased in PAH PASMCs compared to CTL PASMCs (n=4). * $p<0.05$ versus control.

Figure 2. Hyperproliferation of PASMCs is associated with altered acetylation/deacetylation balance.

(A) In PAH PASMCs, SIRT1 mRNA content is unaltered (n=4). (B) Protein levels of SIRT1 and NAMPT in PAH PASMCs do not differ from CTL PASMCs (n=4). (C) The acetylated form of SIRT1 targets histone H1 (n=4) and PGC-1α (n=3) is increased in PAH PASMCs. (D) 24-hour PDGF (10 ng/mL) treatment induces rat PASMC proliferation, as evidenced by the increase in cell number, WST-1 cleavage, BrdU incorporation and proliferating cell nuclear antigen (PCNA) protein level (n=5-6). (E) In rat PASMCs, 24-hour PDGF (10 ng/mL) treatment induces an increase in the acetylated fractions of SIRT1 targets histone H1, FOXO1 (n=4-6) and PGC-1α (n=3) without affecting total protein expression. * $p<0.05$, ** $p<0.01$, *** $p<0.001$ versus respective control.

Figure 3. SIRT1 downregulation favors PASMC hyperproliferation.

(A) SIRT1 silencing by siRNA reduces SIRT1 protein level and increases BrdU incorporation in control human PASMC (n=3). (B) SIRT1 silencing decreases SIRT1 level and increases

PDGF-induced proliferation in rat PASMCs, as evidenced by the increase in cell number, WST-1 cleavage and BrdU incorporation (for BrdU incorporation, p=0.06). SIRT1 protein level reduction shows a trend to increase non-stimulated rat PASMCs proliferation (n=5-6). (C) SIRT1 pharmacological inhibitor sirtinol (5 µmol/L) also facilitates PDGF (10 ng/mL)-induced rat PASMC proliferation (n=7). * p<0.5, ** p<0.01 *versus* respective controls.

Figure 4. SIRT1 downregulation aggravates chronic hypoxia-induced vascular remodeling.

(A) Wild-type SIRT1 protein is significantly reduced in SIRT1 KO mice lungs, in normoxic and hypoxic conditions (n=5-6). SIRT1 downregulation abolishes hypoxia-induced increase in PGC-1α protein content and diminishes the stabilization of HIF-1α protein while augmenting GLUT1 protein content. (n=5-6). (B) Representative images of non muscular, partially muscular and totally muscular vessels. 7-µm lung cryosections are labeled with antibodies against Von Willebrand endothelial factor (VWF) (red) and α smooth muscle actin (αSMA) (green). Nuclei are labeled with Hoechst fluorescent probe (blue). Color merged panels are showed on the right. Chronic hypoxia-induced vascular remodeling is deeper in SIRT1 KO mice lungs, as evidenced by the decrease in the percentage of non muscular vessels, paralleled by an increase in the presence of totally muscular vessels (n=5-6). (C) Right ventricle (RV) pressure elevation is aggravated in SIRT1 KO after hypoxia exposure (n=4-5). Fulton's index, calculated as the ratio of RV weight to the weight of left ventricle (LV) + septum (S), is higher in SIRT1 KO mice compared to WT mice subjected to chronic hypoxia (n=5-6). * p<0.05, ** p<0.01, *** p<0.001 *versus* normoxia; $ p<0.05, $$ <0.01 *versus* wild-type.

Figure 5. SIRT1 activator Stac-3 decreases cell acetylation state and abolishes rat and human PASMCs hyperproliferation

(A) In rat PASMCs, Stac-3 (10 µmol/L) treatment causes a significant reduction of the acetylated levels of SIRT1 targets H1, FOXO1 (n=4-6) and PGC-1α (n=3). Stac-3 also increases NAMPT mRNA content (n=4). (B) Stac-3 strongly inhibits PDGF (10 ng/mL)-induced rat PASMC proliferation, as indicated by the decrease in cell number, WST-1 cleavage by viable cells, BrdU incorporation by replicating cells and proliferating cell nuclear antigen (PCNA) amount, (n=4); (C) SIRT1 specific activator SRT1720 (1 µmol/L) also inhibits rat PASMC proliferation, as evidenced by the significant decrease in WST-1 cleavage (n=6). (D) Stac-3 does not affect rat PASMC mortality: fluorescein diacetate (FDA) negative cells percentage does not increase upon Stac-3 treatment (n=7). The percentage of necrotic cells, permeable to the DNA intercalating probe propidium iodide (PI), is also unchanged (n=4). (E) Stac-3 antiproliferative effect is observed also in human PAH PASMCs by the decrease in WST-1 cleavage, BrdU incorporation, as well as PCNA protein level (n=4). * $p<0.05$, ** $p<0.01$, *** $p<0.001$ *versus* control non-treated PASMCs; $ $p< 0.05$, $$ $p<0.01$ *versus* PDGF-stimulated rat PASMCs or human PAH PASMCs.

Figure 6. SIRT1 activation is associated with a mitochondrial biogenesis enhancement in human and rat PASMCs.

(A) In PAH PASMCs, Stac-3 (10 µmol/L) induces an increase in the protein level of mitochondrial mass markers VDAC and CS in PAH PASMCs (n=3). (B) Stac-3 also increases expression of PGC-1α molecular partners PPARα and ERRα as well as expression of an antioxidant enzyme, SOD2, known to be regulated by PGC-1α (n=4). (C) In rat PASMCs, Stac-3 also increases mitochondrial mass as evidenced by elevation in VDAC and CS protein level; this is accompanied by an increase in mitochondrial transcription factor A (TFAM)

content (n=4-7). (D) Stac-3 activates expression of PGC-1α partners (PPARα, ERRα and NRF2) and of elements of PGC-1α-triggered cascade (TFAM, the antioxidant enzyme glutathion peroxidase 1 (GPx1) and sirtuin3 (SIRT3)) (n=4). * $p<0.05$, ** $p<0.01$, *** $p<0.001$ *versus* control non-treated PASMCs; $ $p< 0.05$, $$ $p<0.01$ *versus* PDGF-stimulated rat PASMCs or human PAH PASMCs.

Figure 7. SIRT1 activation inhibits PDGF-induced mitochondrial fragmentation.
(A) Representative confocal images of rat PASMC mitochondrial network, labeled with MTO (*MitoTracker Orange*). Stac-3 (10 µmol/L) attenuates PDGF (10 ng/mL)-induced mitochondrial fragmentation. (B) Stac-3 prevents PDGF-induced augmentation of the percentage of small mitochondria (≤1 μm^3) and the decrease of highly connected mitochondria (>5 μm^3). Stac-3 also inhibits the tendency ($p=0.059$) of the decrease in the presence of medium-sized mitochondria (between 1 and 5 μm^3). Data are represented as means ± standard errors of four independent experiments. For each experience, at least ten cells per condition are analyzed. * $p<0.05$ *versus* control non-treated PASMCs; $ $p< 0.05$ *versus* PDGF-stimulated rat PASMCs.

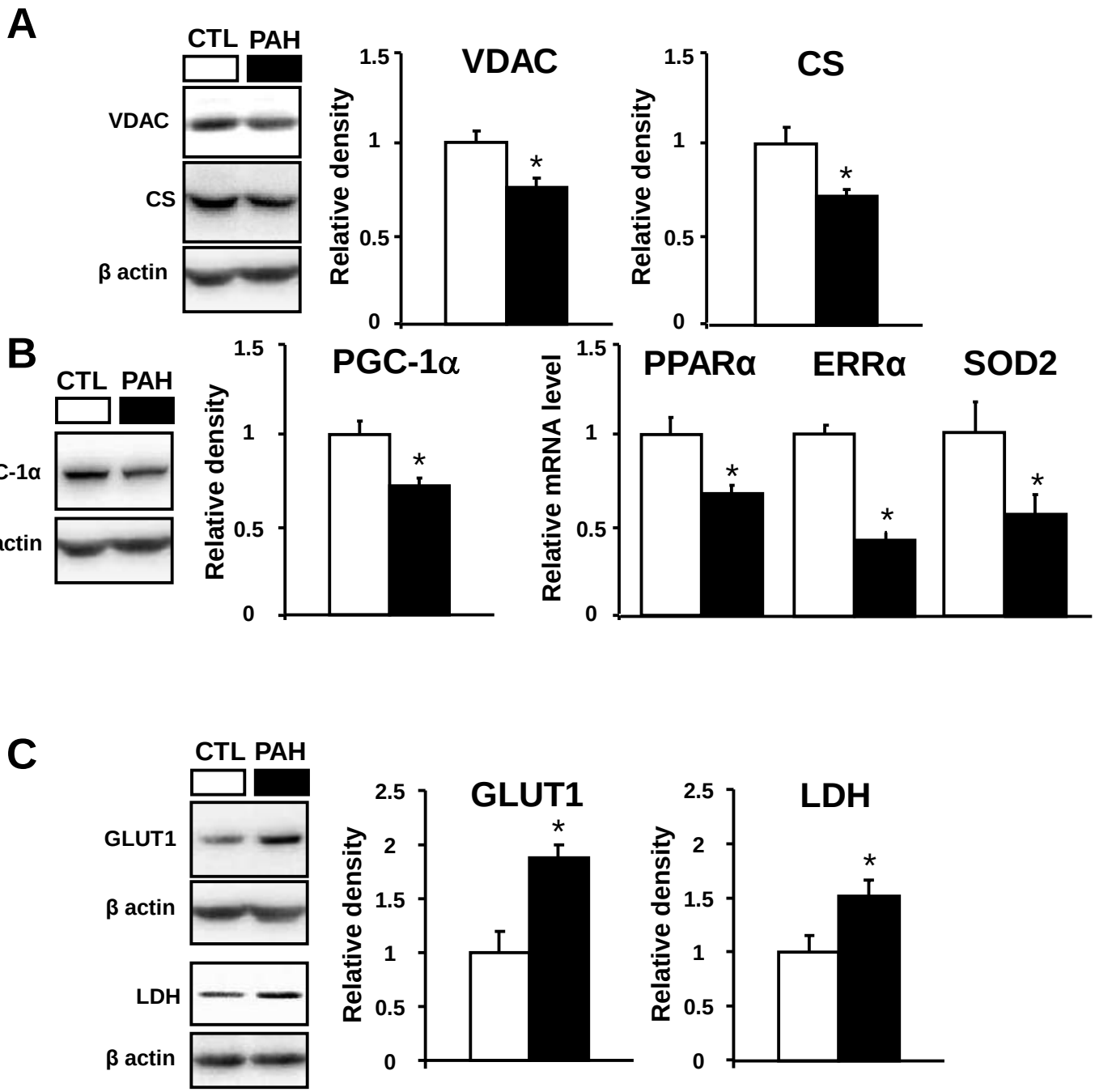
A
CTL
PAH
VDAC
CS
β actin
VDAC
CS
Relative density
1.5
1
0.5
0
*
B
CTL
PAH
PGC-1α
β actin
PGC-1α
PPARα
ERRα
SOD2
Relative density
Relative mRNA level
C
CTL
PAH
GLUT1
β actin
LDH
β actin
GLUT1
LDH
2.5
2
1.5
1
0.5
0

Fig. 1

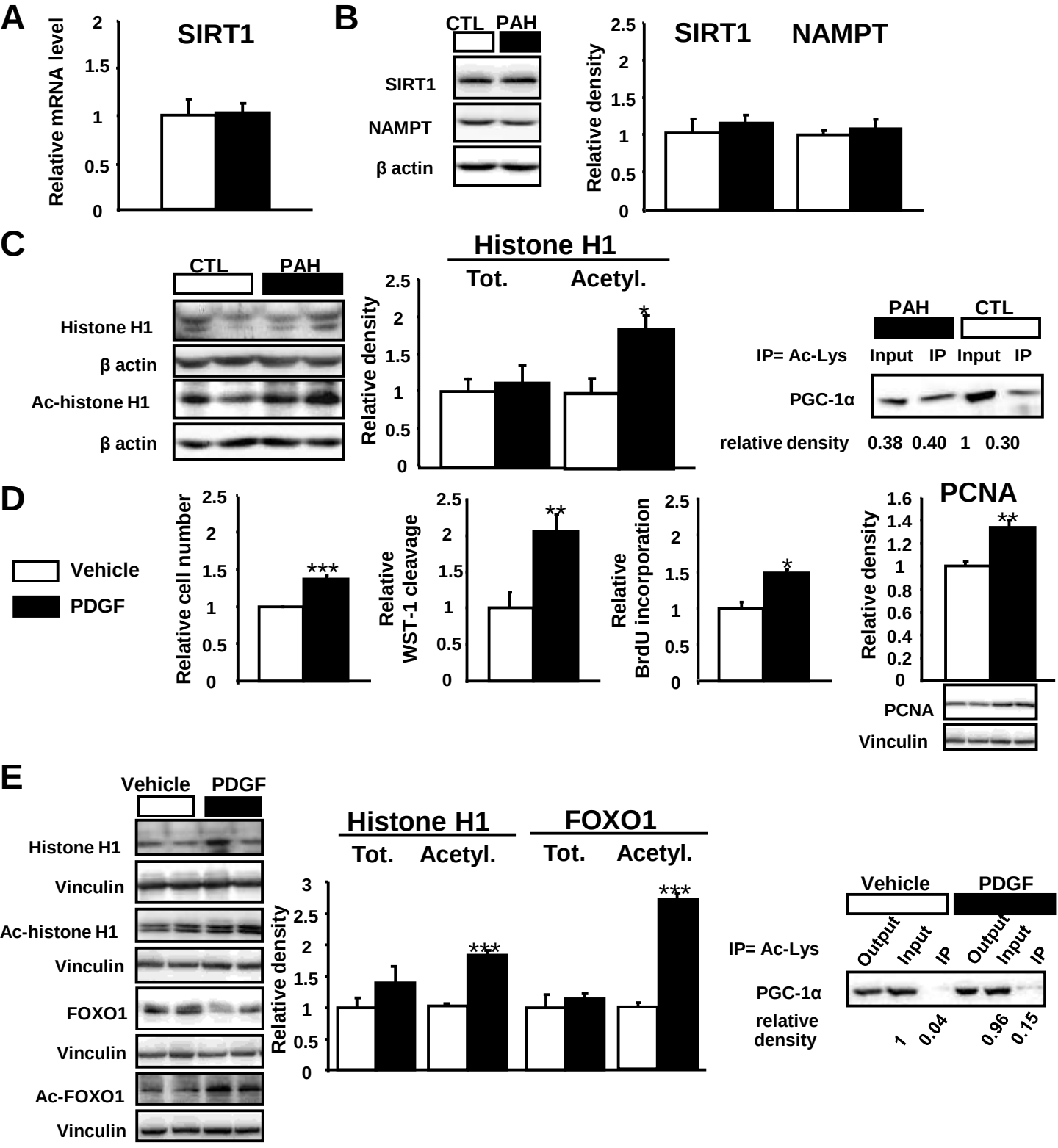
A
SIRT1
Relative mRNA level
2
1.5
1
0.5
0
B
CTL
PAH
SIRT1
NAMPT
β actin
SIRT1
NAMPT
Relative density
2.5
2
1.5
1
0.5
0
C
CTL
PAH
Histone H1
β actin
Ac-histone H1
β actin
Histone H1
Tot.
Acetyl.
Relative density
PAH
CTL
IP= Ac-Lys
Input
IP
Input
IP
PGC-1α
relative density
0.38
0.40
1
0.30
D
Vehicle
PDGF
Relative cell number
Relative WST-1 cleavage
Relative BrdU incorporation
PCNA
Relative density
PCNA
Vinculin
E
Vehicle
PDGF
Histone H1
Vinculin
Ac-histone H1
Vinculin
FOXO1
Vinculin
Ac-FOXO1
Vinculin
Histone H1
FOXO1
Tot.
Acetyl.
Tot.
Acetyl.
Relative density
Vehicle
PDGF
IP= Ac-Lys
Output
Input
IP
Output
Input
IP
PGC-1α
relative density
1
0.04
0.96
0.15

Fig. 2

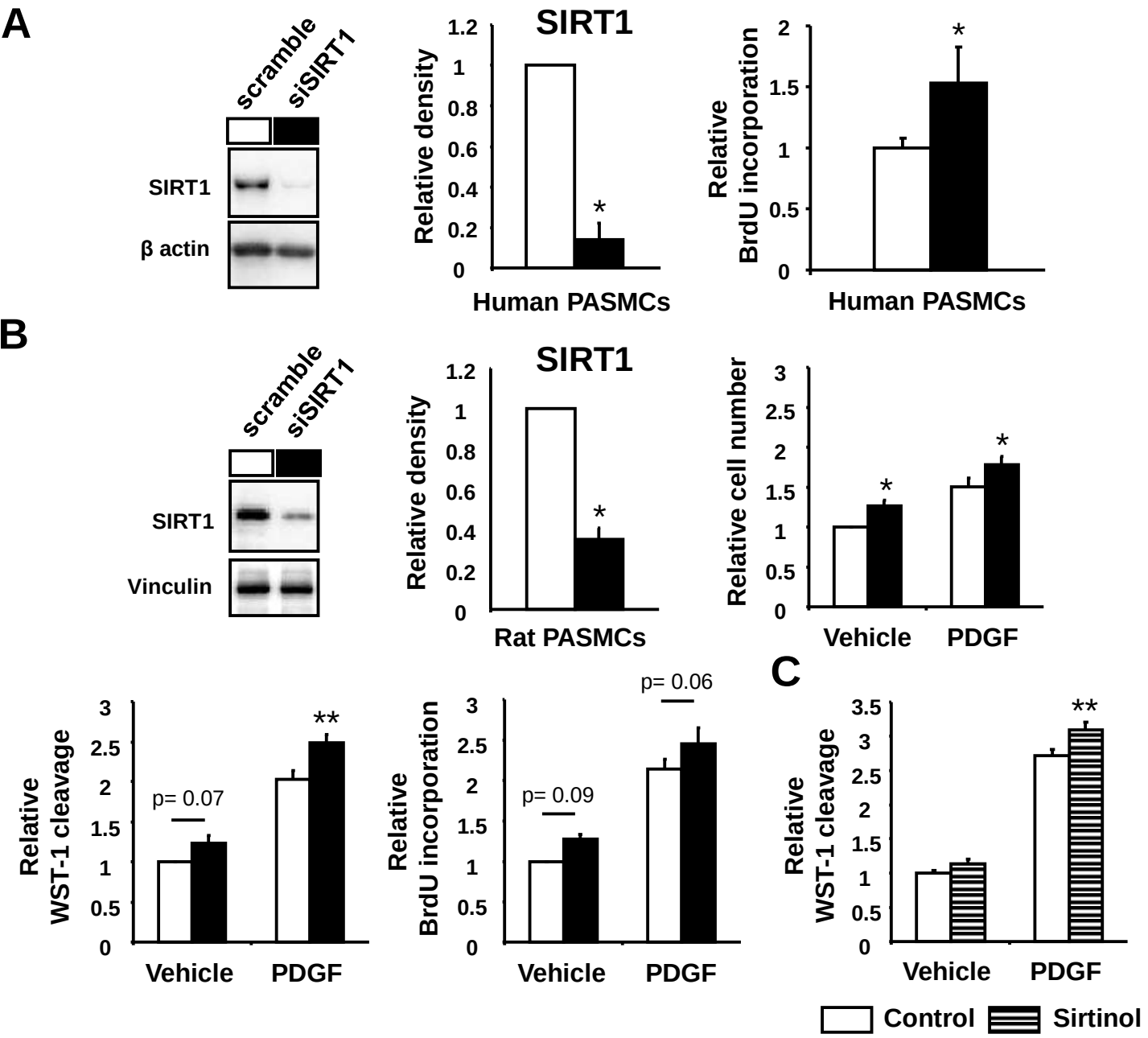
A
scramble
siSIRT1
SIRT1
β actin
SIRT1
Relative density
Human PASMCs
Relative BrdU incorporation
Human PASMCs
B
scramble
siSIRT1
SIRT1
Vinculin
SIRT1
Relative density
Rat PASMCs
Relative cell number
Vehicle
PDGF
Relative WST-1 cleavage
p= 0.07
Vehicle
PDGF
Relative BrdU incorporation
p= 0.09
p= 0.06
Vehicle
PDGF
C
Relative WST-1 cleavage
Vehicle
PDGF
Control
Sirtinol

Fig. 3

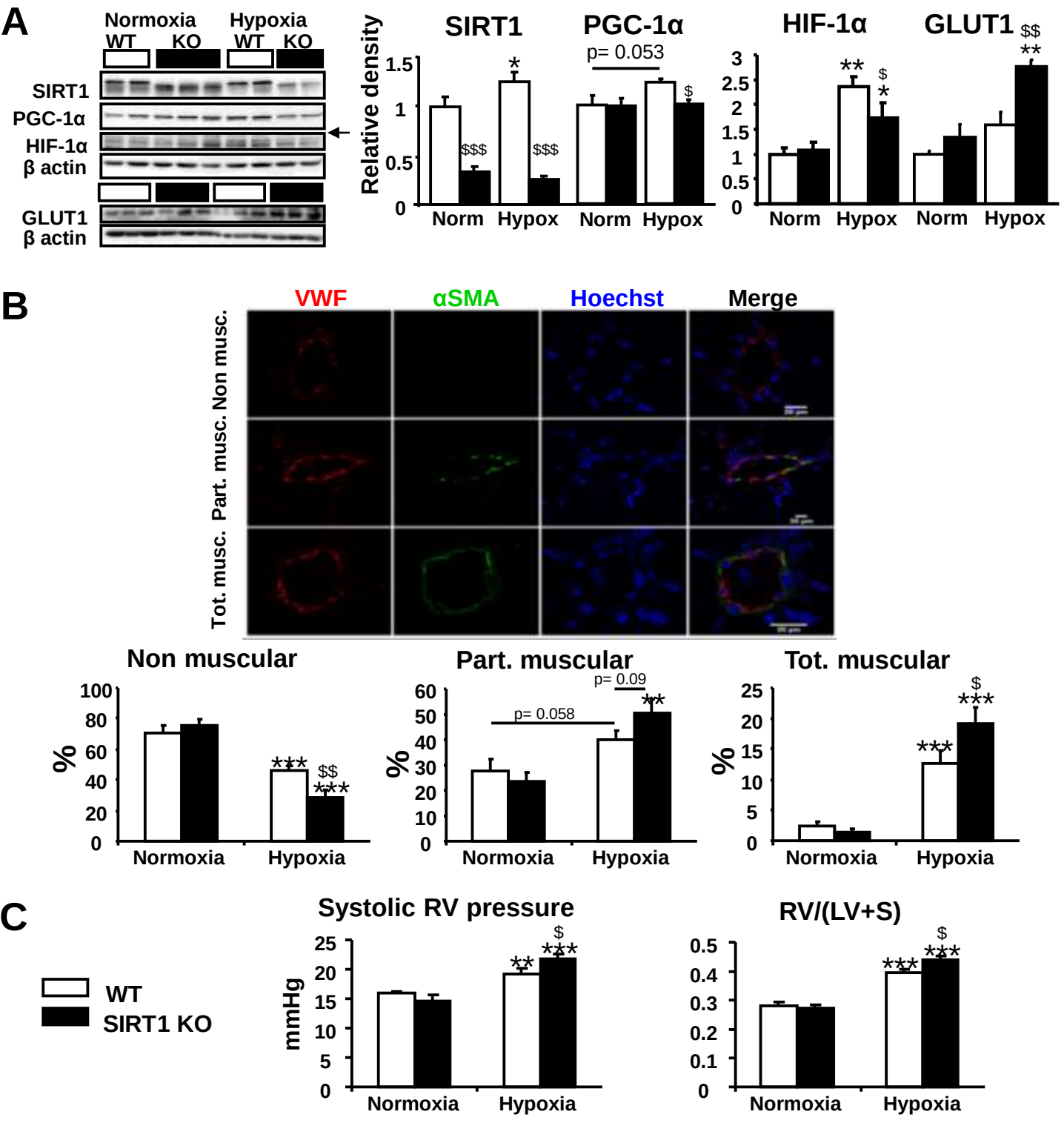
A
Normoxia
Hypoxia
WT
KO
WT
KO
SIRT1
PGC-1α
HIF-1α
β actin
GLUT1
β actin
Relative density
SIRT1
PGC-1α
p= 0.053
HIF-1α
GLUT1
Norm
Hypox
Norm
Hypox
Norm
Hypox
Norm
Hypox
B
VWF
αSMA
Hoechst
Merge
Tot. musc.
Part. musc.
Non musc.
Non muscular
Part. muscular
Tot. muscular
%
p= 0.09
p= 0.058
Normoxia
Hypoxia
C
WT
SIRT1 KO
Systolic RV pressure
mmHg
RV/(LV+S)
Normoxia
Hypoxia

Fig. 4

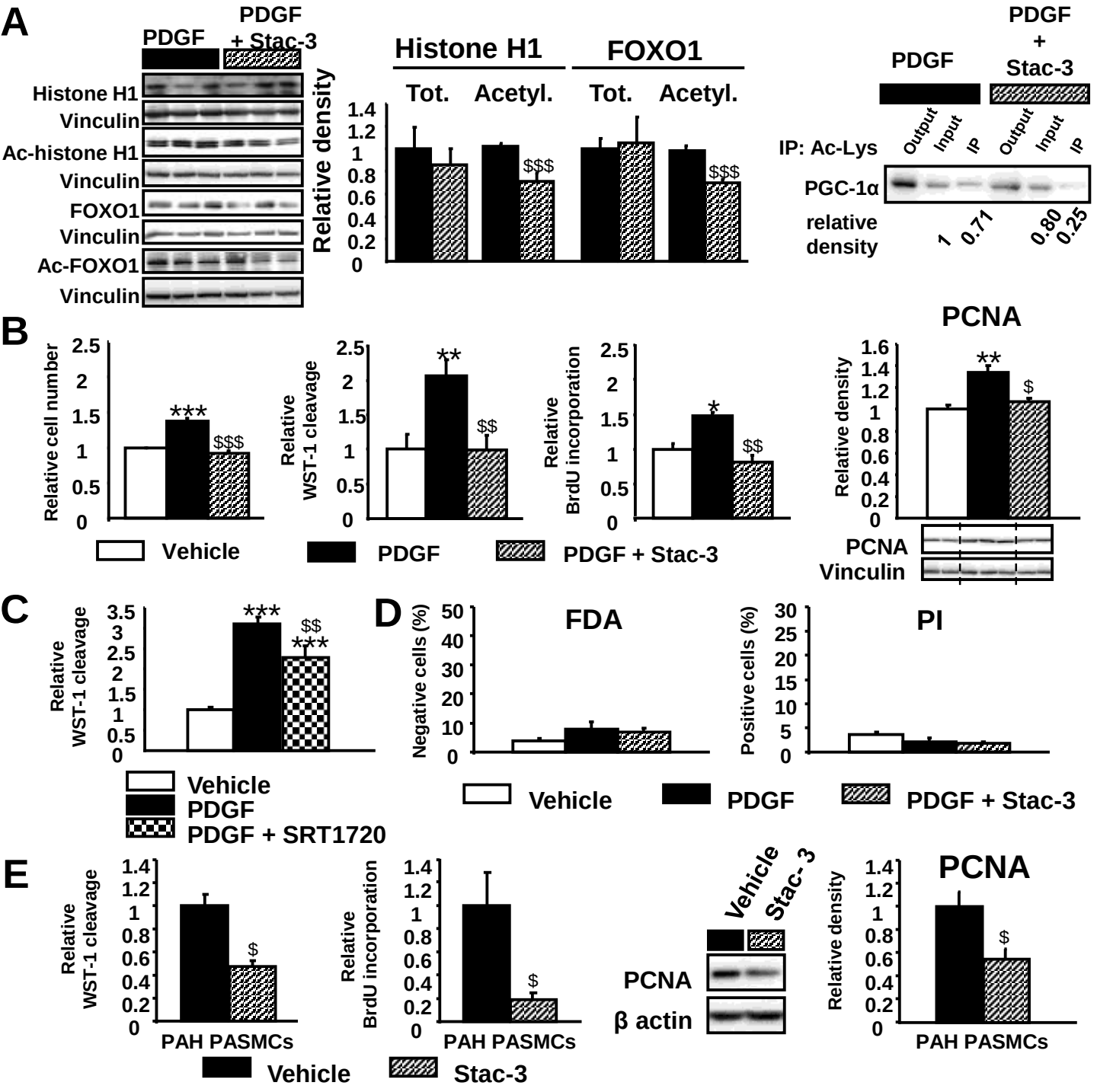
A
PDGF
PDGF + Stac-3
Histone H1
Vinculin
Ac-histone H1
Vinculin
FOXO1
Vinculin
Ac-FOXO1
Vinculin
Relative density
Histone H1
FOXO1
Tot.
Acetyl.
Tot.
Acetyl.
PDGF
PDGF + Stac-3
IP: Ac-Lys
Output
Input
IP
PGC-1α
relative density
1
0.71
0.80
0.25
B
Relative cell number
Relative WST-1 cleavage
Relative BrdU incorporation
PCNA
Relative density
PCNA
Vinculin
Vehicle
PDGF
PDGF + Stac-3
C
Relative WST-1 cleavage
Vehicle
PDGF
PDGF + SRT1720
D
FDA
Negative cells (%)
PI
Positive cells (%)
Vehicle
PDGF
PDGF + Stac-3
E
Relative WST-1 cleavage
PAH PASMCs
Vehicle
Relative BrdU incorporation
PAH PASMCs
Stac-3
Vehicle
Stac-3
PCNA
β actin
PCNA
Relative density
PAH PASMCs

Fig. 5

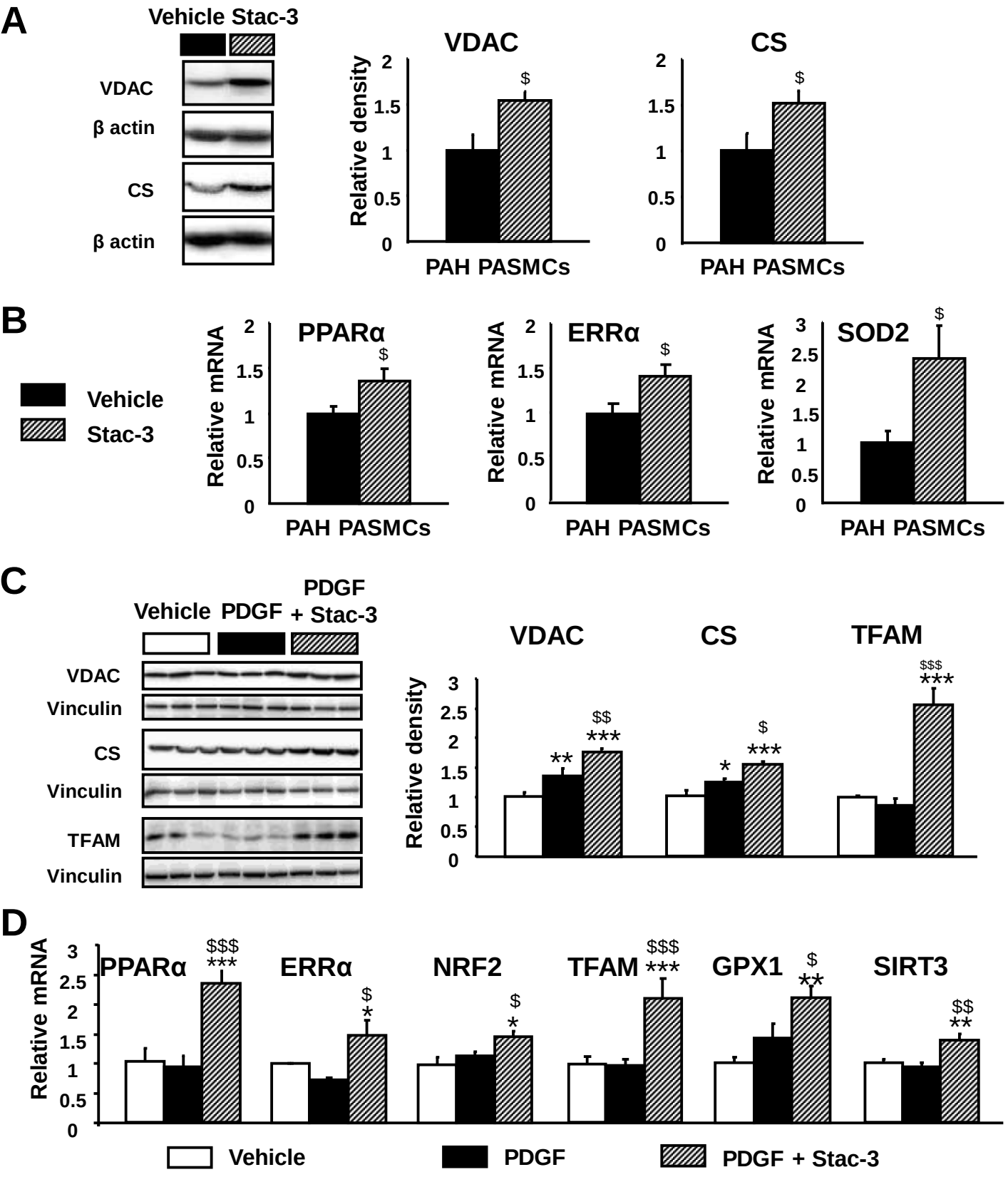
A
Vehicle Stac-3
VDAC
β actin
CS
β actin
VDAC
CS
Relative density
PAH PASMCs
B
Vehicle
Stac-3
PPARα
ERRα
SOD2
Relative mRNA
PAH PASMCs
C
Vehicle
PDGF
PDGF + Stac-3
VDAC
Vinculin
CS
Vinculin
TFAM
Vinculin
VDAC
CS
TFAM
Relative density
D
PPARα
ERRα
NRF2
TFAM
GPX1
SIRT3
Relative mRNA
Vehicle
PDGF
PDGF + Stac-3

Fig. 6

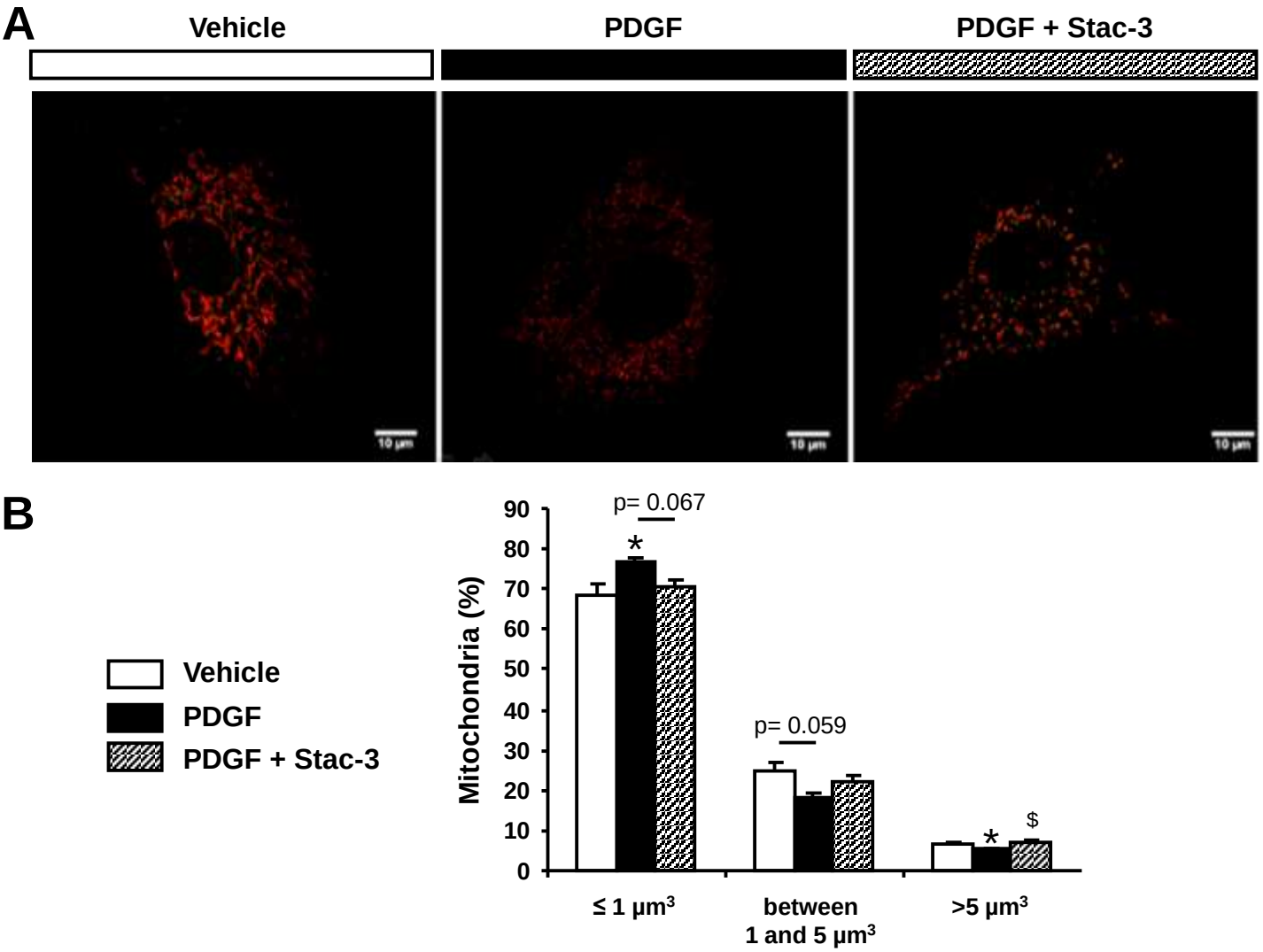
A
Vehicle
PDGF
PDGF + Stac-3
10 µm
10 µm
10 µm
B
Vehicle
PDGF
PDGF + Stac-3
Mitochondria (%)
90
80
70
60
50
40
30
20
10
0
p= 0.067
*
p= 0.059
*
$
≤ 1 µm³
between
1 and 5 µm³
>5 µm³

Fig. 7

Table S1. List of antibodies.

Antibody	Dilution	Manufacturer	Reference
Ac-FOXO	1:500	Santa Cruz, Heidelberg, Germany	sc-49437
Ac-H1	1:1000	Sigma Aldrich, Saint Quentin Fallavier, France	H7789
CS	1:500	Abcam, Cambridge, United Kingdom	ab96600
GLUT1	1:500	Abcam, Cambridge, United Kingdom	ab32551
FOXO	1:1000	Ozyme, Saint Quentin en Yvelines, France	2880S
HIF-1α	1:500	Santa Cruz, Heidelberg, Germany	sc-10790
H1	1:500	Santa Cruz, Heidelberg, Germany	sc-10806
NAMPT	1:250	Abcam, Cambridge, United Kingdom	ab45890
PCNA	1:1000	Santa Cruz, Heidelberg, Germany	sc-56
PGC-1α	1:500	Santa Cruz, Heidelberg, Germany	sc-13067
SIRT1	1:4000	Abcam, Cambridge, United Kingdom	sc-13067
Tfam	1:500	Santa Cruz, Heidelberg, Germany	sc-23588
VDAC	1:1000	Home made	
Vinculine	1:2000	Sigma Aldrich, Saint Quentin Fallavier, France	V9131
β actine	1:10000	Santa Cruz, Heidelberg, Germany	sc-47778

Table S2. Primer sequences.

Gene	Forward primer (5'→3') Reverse primer (5'→3')	Hybridization temperature (°C)
ERRα (human)	CTA TGG TGT GGC ATC CTG TG GTG ATC TCG CAC TCG TTG G	60
ERRα (rat)	TCA AGG AGG GTG TGC GTC TG CTT GGC CCA GCT GAT GGT GA	65
NRF2 (rat)	CAC TCA ACA TTT CGG GAA GAG CTC ATT CAT CTG TTG CTC TTG G	60
GCN5 (human)	CTA TGG GGC AAA CTC TCC AA TCC AGA CTC AGG GAG CTG TT	60
GPX1 (rat)	GTT TCC CGT GCA ATC AGT TC TCA CTT CGC ACT TCT CAA ACA	60
NAMPT (rat)	TGA ATT GCT CCT TCA AGT GC TTT GTT GGG ATC AGC AAC TG	60
PPARα (human)	CCT CTC AGG AAA GGC CAG TA CAG TGA AAG ATG CGG ACC TC	60
PPARα (rat)	ATG AGT CCC CTG GCA ATG GGC ATT CTT CCA AAA CGG	58
RPLP0 (human)	GCG ACC TGG AAG TCC AAC TA TTG TCT GCT CCC ACA ATG AA	60
RPLP2 (rat)	GCT GTG GCT GTT TCT GCT TC ATG TCG TCA TCC GAC TCC TC	62
RPL4 (human)	GCA AGC TGA ACA TTT TGA TTG GAT CTC TGG GCT TTT C	61
RPL32 (human, rat)	GCT GCT GAT GTG CAA CAA A GGG ATT GGT GAC TCT GAT GG	60
SIRT1 (human)	ATT TAT GCT CGC CTT GCT GT CCA GCG TGT CTA TGT TCT GG	60
SIRT3 (rat)	TAC ATG CAC GGT CTG TCG AA ACA ACG CCA GTA CAG ACA GG	60
SOD2 (human)	CGT CAC CGA GGA GAA GTA CC AGT CAC GTT TGA TGG CTT CC	60
TBP (human, rat)	AAA GAC CAT TGC ACT TCG TG GCT CCT GTG CAC ACC ATT TT	60
Tfam (rat)	GAA AGC ACA AAT CAA GAG GAG CTG CTT TTC ATC ATG AGA CAG	60
YWHAZ (rat)	AGA CGG AAG GTG CTG AGA AA GAA GCA TTG GGG ATC AAG AA	60

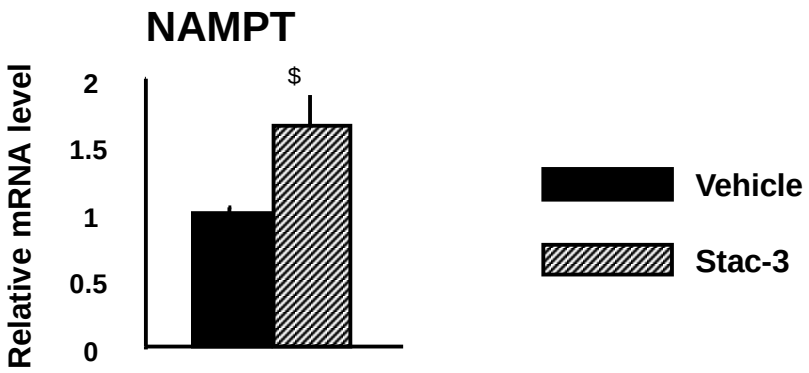

Fig. S1. SIRT1 activation by Stac-3 increases the NAMPT (nicotinamide phosphoribosyltransferase) gene expression in rat PASMCs.

$ - P<0.05